J Solid State Electrochem (2009) 13:959–965
DOI 10.1007/s10008-008-0624-1

ORIGINAL PAPER

Oxygen evolution on $Ru_{1-x}Ni_xO_{2-y}$ nanocrystalline electrodes

Kateřina Macounová · Jakub Jirkovský · Marina V. Makarova · Jiří Franc · Petr Krtil

Received: 2 January 2008 / Revised: 2 July 2008 / Accepted: 7 July 2008 / Published online: 14 August 2008

Abstract Nanocrystalline $Ru_{1-x}Ni_xO_{2-y}$ with $0.02<x<0.30$ were prepared by a sol–gel approach at temperatures between 300 and 600 °C. XRD patterns of the prepared materials indicate a single-phase character conforming to a tetragonal syngony. All prepared materials are sufficiently stable in acid media and show activity towards oxygen evolution. The activity towards oxygen evolution reaction of the materials with constant chemical composition decreases with increasing particle size. The increasing Ni content enhances the electrocatalytic activity in a stepwise manner with abrupt changes for materials containing approximately 5% or 15% of the cationic sites substituted by Ni.

Introduction

The oxygen evolution reaction (OER) on oxide surfaces is in the focus of electrochemical research for more than three decades mainly due to its importance in industrial electrolytic processes. The most popular oxide electrocatalysts for OER represent nanocrystalline forms of transition metal oxides with rutile (e.g. RuO_2, IrO_2) [1] or spinel structure (e.g. Co_3O_4) [2] or transition metal oxohydroxide with layered structure like, e.g. NiOOH [3] or MnOOH [4]. The rutile structure oxides are primarily targeted for acid media and the spinel structure and oxohydroxides, on the other hand, for alkaline media. The favourable thermodynamics of the oxygen evolution on the oxide electrocatalysts, namely, on those with rutile structure, was recently rationalised by means of DFT calculations for (111)-oriented single crystal faces [5]. The behaviour of real nanocrystalline systems can, however, differ, since these materials contain a high number of crystal edges and vertices, the behaviour of which is not reflected in theoretical calculations.

The oxygen evolution process in acid media can be seen as the consecutive removal of one electron from chemisorbed oxygen on the electrode surface (see Eqs. 1, 2, 3 and 4) [6]:

$$S + H_2O \rightarrow S - OH + H^+ + e^-, \quad (1)$$

$$S - OH \rightarrow S - O + H^+ + e^-, \quad (2)$$

$$S - OH + S - OH \rightarrow S - O + S + H_2O, \quad (3)$$

$$S - O + S - O \rightarrow O_2 + 2S. \quad (4)$$

The S in the reaction scheme represents an active site on the electrode surface, the nature of which is unknown. The oxygen evolution on nanocrystalline oxide electrocatalysts is particle size/shape-sensitive. The crystals edges on the prismatic part of the RuO_2 nanocrystals [7, 8] were reported to be the primary sites for surface oxygen recombination. The effect of the particle size may be suppressed in the case of hetero-static substitution (e.g. RuO_2 doped by Co), the actual origin of this behaviour remains unknown [8].

This paper extends previous studies describing particle size and chemical composition dependence of the oxygen evolution on nanocrystalline electrocatalysts derived from

K. Macounová · J. Jirkovský · M. V. Makarova · J. Franc · P. Krtil (✉)
J. Heyrovský Institute of Physical Chemistry,
Academy of Sciences of the Czech Republic,
Dolejškova 3,
18223 Prague, Czech Republic
e-mail: Petr.Krtil@jh-inst.cas.cz

RuO_2 to the previously unexplored Ru–Ni–O system, which can provide significantly broader range of compositions in which the materials give single-phase nanocrystals in comparison to, e.g. the Ru–Co–O system [8]. Electrochemical and X-ray diffraction data are combined to outline both chemical composition and particle size role in the electrocatalytic activity of nanocrystalline $Ru_{1-x}Ni_xO_{2-y}$ towards oxygen evolution.

Experimental

The ruthenium dioxide and $Ru_{1-x}Ni_xO_{2-y}$ samples were prepared using a sol–gel approach [7, 9]. For $Ru_{1-x}Ni_xO_{2-y}$ samples, a starting solution of ruthenium(III) nitrosylnitrate (98%, Alpha Aesar) and nickel (II) nitrate in mixture (1:1) of ethanol and propane-2-ol (both Aldrich, ACS grade) were precipitated with aqueous solution of tetramethylammonium hydroxide (25% Alpha Aesar). The starting solutions containing both Ru and Ni were characterised by the Ru/Ni ratio shown in Table 1. After precipitation, the formed amorphous precursors were aged in PTFE-lined stainless steel autoclaves at 100 °C for 40 h to facilitate the filtration process. The filtered amorphous precipitates were re-crystallised at temperatures above 300 °C in air for 4 h to obtain nanocrystalline morphology. The crystallinity and phase purity of the prepared samples was checked using Bruker D8 Advance powder X-ray diffractometer with Vantec-1 detector and CuKα radiation. The information about the characteristic particle size of the prepared nanocrystals (and morphology of the related electrodes—vide infra) was assessed by means of scanning electron microscopy using field emission scanning electron microscope (SEM) Hitachi S4800 equipped with an EDX detector (Thermo Noran).

The electrodes for electrochemical experiments were prepared from synthesised RuO_2 and $Ru_{1-x}Ni_xO_{2-y}$ materials by sedimentation of powder from a water-based suspension on Ti mesh (open area 20%, Goodfellow). The oxide suspension contained approximately 5 g/L of ruthenium-based oxide in MilliQ quality de-ionised water. The duration of the deposition was adjusted to obtain the surface coverage of about 1–2 mg/cm^2 of active oxide. The actual mass of the electrocatalysts for each electrode was determined by weighting the substrate before and after the deposition process. To improve the mechanical stability of electrodes, the deposited layers were later annealed for 20 min at 400 °C in air.

Table 1 Ru/Ni ratio, particle size and elementary cell volumes for $Ru_{1-x}Ni_xO_{2-y}$ oxides with different Ni content

x	Ru/Ni	D (nm)	V (Å^3)
0.02	49:1	45	62.638
0.05	19:1	53	62.436
0.10	9:1	66	62.358
0.15	17:3	71	62.370
0.20	4:1	125	62.435
0.25	3:1	126	62.503
0.30	7:3	122	62.539

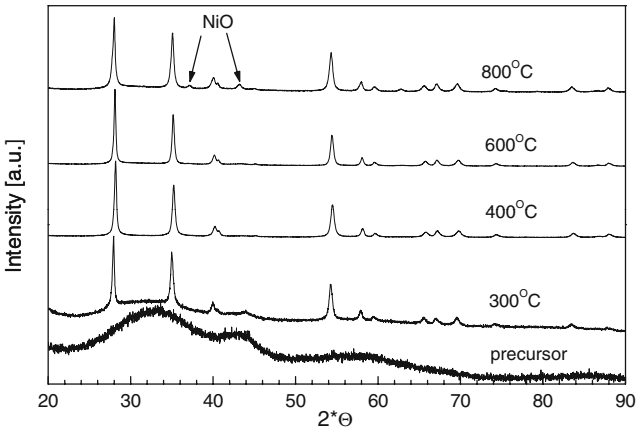

Fig. 1 Powder X-ray diffractograms of $Ru_{0.8}Ni_{0.2}O_{2-y}$ annealed at different temperatures. The actual annealing temperature is shown in the figure legend

The electrocatalytic activity of the prepared materials with respect to oxygen evolution was studied in an acid solution containing 0.1 M $HClO_4$ by cyclic voltammetry. All experiments were performed in a home-made Kel-F single compartment cell using a three-electrode arrangement controlled by a PAR 263A potentiostat. Pt and saturated calomel electrode (SCE) were used as auxiliary and reference electrode, respectively. All potentials shown in the text are quoted with respect to SCE. The DEMS apparatus consisted of the Prisma™ QMS200 quadrupole mass spectrometer (Balzers) connected to the TSU071E turbomolecular drag pumping station (Balzers).

Result and discussion

Solid state characterisation

The XRD patterns of all prepared phases are of single-phase character and can be indexed on the basis of rutile type structure (P_{42}/mnm). In contrast to substitution with Co [10] in which case the single-phase material was reported for single chemical composition (with 20% substitution in cationic sub-lattice), Ni seems to be better compatible with rutile structure. X-ray diffraction patterns of the $Ru_{1-x}Ni_xO_{2-y}$ samples conform to a single phase in concentration range corresponding to occupancy of cationic

sites by Ni from 2% to 30%. It needs to be noted that the materials annealed at the lowest temperatures may contain a small amount of residual amorphous phase. As in the case of materials doped with Co [10], the Ni-substituted phases are meta-stable and decompose to Ru-rich tetragonal phase and nanocrystalline NiO at temperatures above 600 °C (see Fig. 1). The Rietveld analysis of the measured diffraction patterns shows a complex dependence of the crystal structure on the average Ni content. The unit cell volume first decreases with increasing Ni content, passes through a minimum and increases with increasing Ni content for materials with Ni content higher than 10% (see Table 1). The characteristic particle size of the prepared materials determined by statistical evaluation of 150 randomly selected particles in the SEM micrographs (see Fig. 2) increases with increasing annealing temperature (see Table 1). The resulting particle size of the $Ru_{1-x}Ni_xO_{2-y}$ nanocrystals is bigger than that of the RuO_2 nanocrystals prepared at similar conditions. In addition to it, the prepared materials tend to be composed of two characteristic particle sizes if the concentration of incorporated Ni exceeds approximately 15% of the cationic sites. The $Ru_{1-x}Ni_xO_{2-y}$ particle size

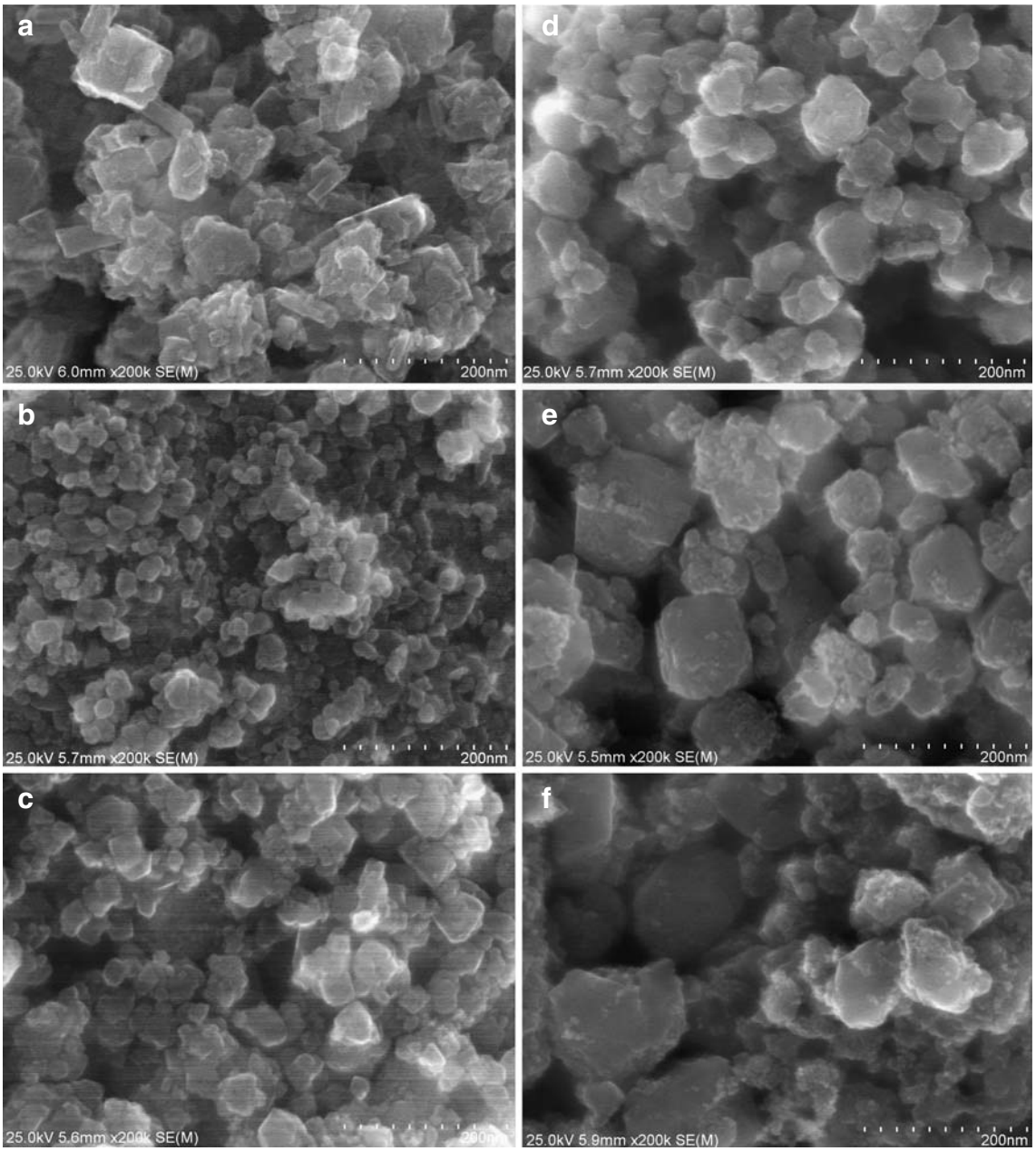

Fig. 2 SEM images of the nanocrystalline electrodes prepared from $Ru_{1-x}Ni_xO_{2-y}$ powders where x equals to **a** 0.00, **b** 0.02, **c** 0.05, **d** 0.10, **e** 0.15 and **f** 0.20

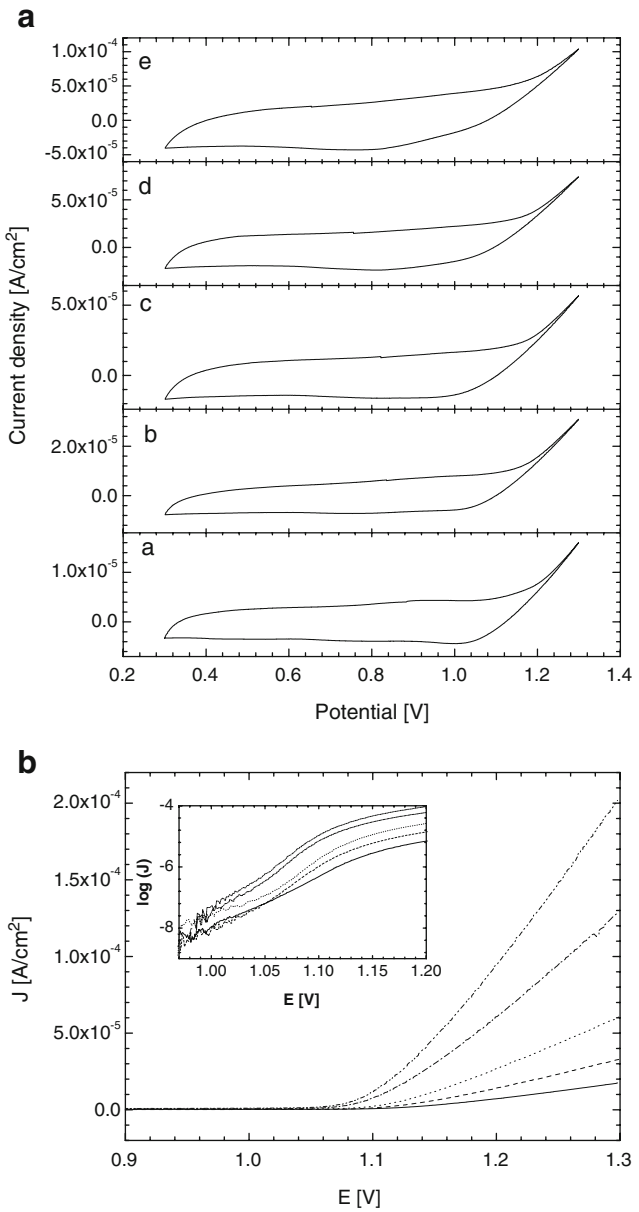

Fig. 3 **a** Typical voltammograms corresponding to the pseudocapacitive behaviour of the $Ru_{1-x}Ni_xO_{2-y}$ electrodes (x ranging between 0 and 0.20) in 0.1 M $HClO_4$ solution at a polarisation rate of 100 mV/s. The actual x values are as follows: 0 (*a*), 0.02 (*b*), 0.05 (*c*), 010 (*d*) and 0.20 (*e*). **b** Oxygen evolution in 0.1 M $HClO_4$ on nanocrystalline RuO_2 electrode (average particle size 34 nm) (*solid line*) and nanocrystalline $Ru_{1-x}Ni_xO_{2-y}$ electrodes with variable Ni content recorded at a polarisation rate of 1 mV/s. The actual Ni content was as follows: x= 0.02 (*dashed line*), x=0.1 (*dotted line*), x=0.2 (*dot and dash line*) and 0.3 (*dot, dot and dash line*). The figure *inset* shows the voltammetric data in logarithmic form used in Tafel analysis. The curve assignment of the inset is the same as for the main figure

can be, therefore, controlled by two factors—annealing temperature and average Ni content. The nanocrystal size increases with increasing Ni content; the same trend can be ascribed to the annealing temperature if the Ni content of the material remains constant.

Electrocatalytic activity

The electrocatalytic activity of the prepared $Ru_{1-x}Ni_xO_{2-y}$ phases was studied for oxygen evolution in acid media in the absence of strongly adsorbing anions. Typical voltammograms of nanocrystalline RuO_2 and $Ru_{1-x}Ni_xO_{2-y}$ electrodes recorded in 0.1 M $HClO_4$ are shown in Fig. 3. It needs to be noted that comparison of the voltammetric data directly obtained in the experiment may be misleading since the studied electrocatalysts feature different characteristic particle size. Due to this possible source of ambiguity, we decided to relate the measured voltammetric data to actual physical area of the electrocatalyst which was determined from known electrocatalyst mass and characteristic particle size (assuming a spherical approximation of the particle shape). The presented current densities are, therefore, by two to three orders of magnitude smaller than those related to projected geometric area of the electrodes (which are of the order of 0.001 to 0.01 $mAcm^{-2}$). As follows from the cyclic voltammograms shown in Fig. 3, the substitution of Ru by nickel has no pronounced effect on the electrochemical behaviour in the double-layer region. The recorded voltammograms are qualitatively the same as that observed on undoped RuO_2 prepared by a similar synthetic technique. The measured voltammograms do not change significantly with time. Such a behaviour may be taken as an indicator of the relative chemical stability of the Ni-doped RuO_2. The EDX analysis of the electrocatalysts composition did not show significant deviation in the Ru/Ni ratio on the time scale of 10^5 s (see Fig. 4). Also, the electrolyte solution was found to be Ni-free after electrochemical experiments. It needs to be noted that the stability interval supported by the available

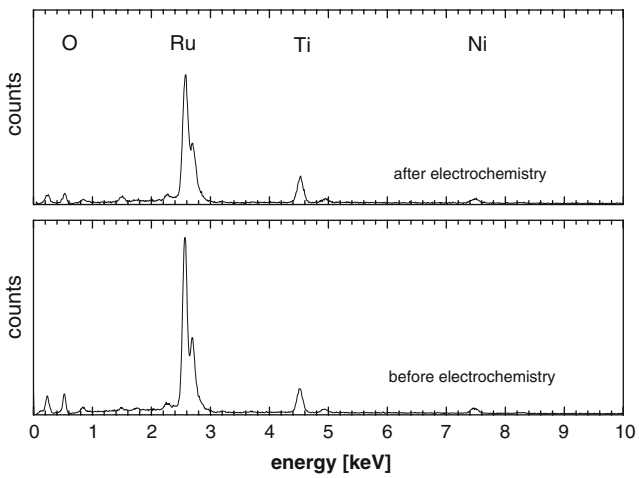

Fig. 4 EDX spectra of the $Ru_{0.9}Ni_{0.1}O_{2-y}$ electrode before and after electrochemical experiments. Individual emission lines are indicated in the figure legend

data is sufficient for the common electroanalytical testing. It bears no comparison, however, with the stability time scale required for industrial applications (10^8 s).

The current increase recorded at potentials positive to 1.0 V can be attributed to the oxygen evolution process.

The particle size effect

The effect of the average particle size on the onset of the exponential current increase attributable to oxygen evolution and overall activity (expressed as the exchange current density and current density at 1.20 V) on nanocrystalline RuO_2 and $Ru_{0.8}Ni_{0.2}O_{2-y}$ is shown in Fig. 5. Figure 5 illustrates that, regardless of the presence of the doping cation, the onset of the oxygen evolution shifts towards more positive potentials with increasing particle size. The shift in the onset potential is accompanied with a drop in the overall electrocatalytic activity. Such a trend in electrocatalytic behaviour seems to support different reactivity of the crystal faces and crystal edges of nanocrystalline RuO_2 proposed for oxygen evolution [7]. The proposed model assumes nanocrystal edges, in particular those separating {100} and {110} crystal faces, to be primary sites of the recombination of molecular oxygen at the electrode surface [7]. Although a detailed analysis of the $Ru_{1-x}Ni_xO_{2-y}$ nanocrystal shape is not available at the moment, we may envisage that the fraction of atoms (which may form active sites for oxygen evolution) at the crystal edges decreases with increasing particle size resulting in the observed decrease of electrocatalytic activity and a shift of the oxygen evolution towards higher potentials.

Table 2 Tafel slope b recorded for the oxygen evolution on $Ru_{1-x}Ni_xO_{2-y}$ electrodes in 0.1 M $HClO_4$ at polarisation rate of 1 mV s^{-1}

x	b (mV/decade)
0.02	53
0.05	53
0.10	53
015	47
0.20	41
0.25	48
0.30	49

Chemical composition effect

The voltammograms presented in Fig. 3b can be subject to Tafel analysis (see inset to Fig. 3b) providing us with Tafel slope and exchange current density values which may be used to characterise the role of the different electrode materials on the oxygen evolution processes. The Tafel slopes obtained by analysis of the data shown in Fig. 3b are summarised in Table 2. The data listed in Table 2 are practically independent of the actual Ni content and range between 48 and 52 mV/decade. These values are slightly higher than those reported for the conventional RuO_2 anodes previously [8]. The constant value of the Tafel slope indicates that the actual Ni content has a negligible effect on the rate-limiting step of the electrode process.

The effects of the change of the Ni content on the onset of the oxygen evolution and electrocatalytic activity of $Ru_{1-x}Ni_xO_{2-y}$ are summarised in Fig. 6. The onset potential of the oxygen evolution shows a continuous shift towards

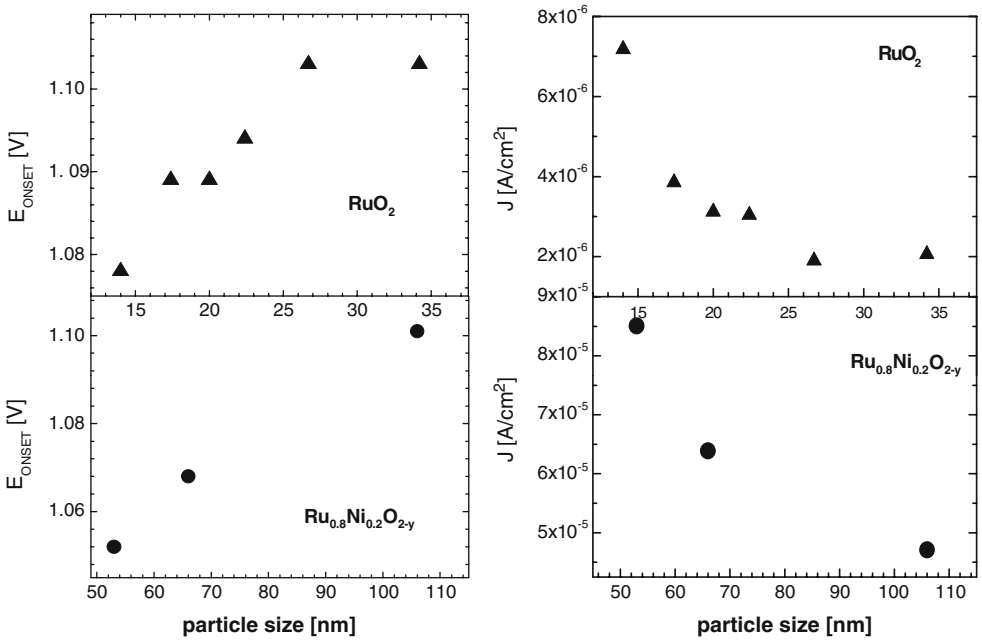

Fig. 5 Potentials of the oxygen evolution onset (*left*) and electrocatalytic activity (*right*) as a function of the particle size for RuO_2 (*top*) and $Ru_{0.8}Ni_{0.2}O_{2-y}$ (*bottom*) electrode oxygen evolution materials. The experimental conditions were the same as in the Fig. 2

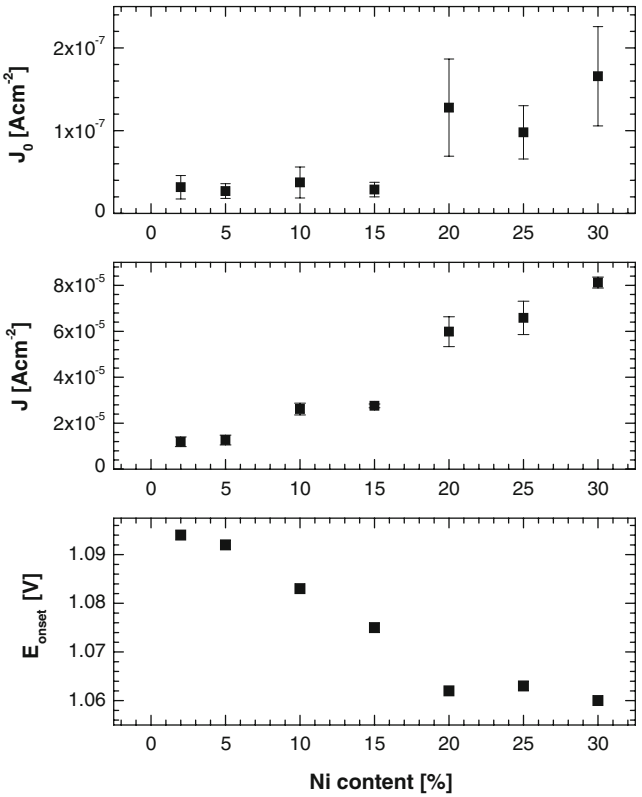

Fig. 6 The potentials of the oxygen evolution onset, exchange current density and current density corresponding to oxygen evolution at $Ru_{1-x}Ni_xO_{2-y}$ at 1.2 V as a function of Ni content. The presented data were extracted from experiments done at a polarisation rate of 1 mV/s in 0.1 M $HClO_4$

lower potentials with increasing Ni content and reaches a plateau at approximately 1.06 V when the Ni content reaches approximately 20%. The Ni content dependence of the overall electrocatalytic activity of $Ru_{1-x}Ni_xO_{2-y}$ materials is also generally increasing with increasing Ni content. This tendency can be demonstrated by both exchange current density and current density observed at potential departed by approximately 300 mV from the standard potential for oxygen evolution (1.2 V vs. SCE). In the case of the exchange current density, one can describe the observed Ni content-related increase as polynomial or exponential. It needs to be noted that the Ni content effect on the measured current density at 1.2 V, although it gives generally increasing dependence, conforms rather to discontinuous stepwise increases in the observed electrocatalytic activity. These abrupt changes were observed for materials the cationic sub-lattice of which was substituted by Ni from approximately 10% and/or 20%, respectively. In the composition intervals marked by these compositions, the OER-related activity of $Ru_{1-x}Ni_xO_{2-y}$ oxides seems to be little affected by the actual change in the Ni content. The materials with Ni content below x=0.05 show electrocatalytic activity comparable to that of the nanocrystalline RuO_2. In the case of $Ru_{1-x}Ni_xO_{2-y}$ oxides with x ranging between 0.05 and 0.15, one observes specific electrocatalytic activity independent of the Ni content; its value is, however, higher than that of the nanocrystalline RuO_2 of comparable particle size.

Analysing the observed electrocatalytic activity values, one has to realise the absence of explanation for the polynomial/exponential increase of the electrocatalytic activity with linear increase of the Ni content. The observed

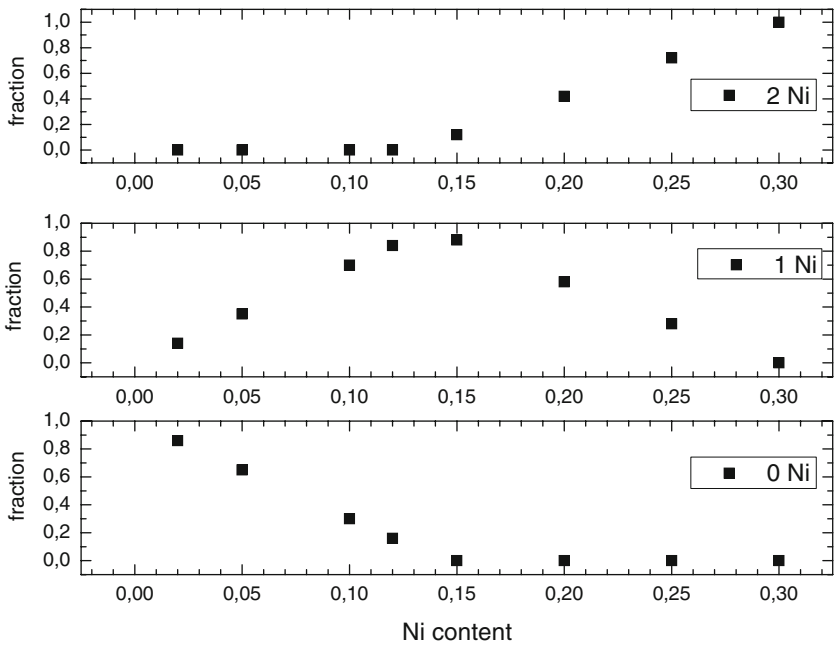

Fig. 7 Distribution of different active sites at the {110} oriented surface as a function of total Ni content

trend, therefore, suggests that the electrocatalytic activity is not directly proportional to the number of Ni atoms on or near the electrode surface and that the present Ni affects the electrocatalytic behaviour of the oxide rather via cation–cation interactions. Such a fact makes the rationalisation of the Ni content-related effect a rather difficult task. Even if we adopt several simplifying assumptions (like, e.g. that the incorporated Ni is uniformly distributed in the structure), one has to reflect the fact that the variation in Ni content yields materials differing both qualitatively as well as quantitatively. With respect to the fact that the major cation in the studied materials is ruthenium, one can relate the observed behaviour to different types of Ru atoms and their abundance in dependence on the total Ni content. By different Ru atoms, we understand atoms present in local environment differing within first two coordination shells [11]. To keep our analysis on rudimentary level, one may adopt a simplified approach neglecting some details of the rutile structure—namely, we can approximate the first coordination shell with an octahedron and assume the same probability for the presence of Ni in any site of the second coordination shell. These simplifications give us a chance to predict the presence of three different Ru atoms in the studied materials, the abundance of which will change with the change of the overall Ni content. The effect of the overall Ni content on the abundance of these Ru coordinations is depicted in Fig. 6. The model depicted in Fig. 7 predicts that the Ru–Ni–O oxides containing less than 20% of Ni contain Ru in two qualitatively different local environments—one containing no Ni in the second coordination shell (further denoted as A) and in such when the second coordination shell of the Ru contains exactly one Ni atom (further denoted as B). The situation gets qualitatively changed when the Ni content exceeds 20% when the Ru in A environment vanishes and a new local environment, further denoted as C (in which the second coordination shell surrounding the Ru contains two Ni atoms) appears. It may be also envisaged that the Ru atoms with different local structures will generally exhibit different electrocatalytic activities in the OER. The overall electrocatalytic activity (which can be extracted from the experiments), therefore, reflects both specific activity of the given Ru in a particular local environment and its abundance on the surface. Despite the fact that there is no information on the specific activity of each of such site, one can expect, in general, a discontinuous change in the electrocatalytic activity when the surface of the oxide starts to contain Ru in qualitatively different environments. Such changes are predicted for materials containing 2% and 20% of the cationic sites substituted by Ni (see Fig. 7). It needs to be noted that the observed discontinuities on the plots shown in Fig. 6 coincide with the expected changes based on the above outlined model. This coincidence cannot be taken, however, as a conclusive proof and more sophisticated approach involving, e.g. X-ray absorption spectroscopy, needs to be adopted to test the adequateness of such an explanation.

Conclusions

A series of nanocrystalline solid solutions conforming to a formula $Ru_{1-x}Ni_xO_{2-y}$ exists within the composition interval $0.02 \leq x \leq 0.3$. Prepared mixed oxides show a tetragonal structure of rutile type. The increasing Ni content has minor effect on the crystalline structure of the Ru–Ni–O oxides. The electrocatalytic activity for oxygen evolution of $Ru_{1-x}Ni_xO_{2-y}$ is controlled by particle size and total Ni content. In the case of materials of constant chemical composition and varying particle size, the particle size controls the OER-related activity which decreases with increasing particle size. This behaviour agrees with that reported for previously studied RuO_2 nanocrystals prepared by a similar synthetic approach and reflects most likely the role of crystal edges on prismatic parts of nanocrystals which are the primary sites for oxygen recombination [7]. The role of the Ni content in the electrocatalytic OER process is more complex. The Ni acts most likely via cation–cation interactions within secondary coordination shells of the surface-confined Ru. The interactions between Ni and Ru in these shells enhance the electrocatalytic activity of the materials towards oxygen evolution; the activity increase seems to be increasing with increasing number of Ni atoms within the secondary coordination shell. This results in a rather discreet increase of the OER activity of the Ru–Ni–O oxides when the total Ni content exceeds 5% and 15%.

Acknowledgement This work was supported by the Academy of Sciences of the Czech Republic under contract no. KAN100400702.

References

1. Trastti S (2000) Electrochim Acta 45:2377
2. Iwakura C, Honji A, Tamura H (1981) Electrochim Acta 26:1319
3. Kibria MKF, Mridha MS (1996) Int J Hydrogen Energy 21:179
4. El-Deab MS, Awad MI, Mohammed AM, Ohsaka T (2007) Electrochem Commun 9:2082
5. Rossmeisl J, Qu ZW, Zhu H, Kroes G-J, Nørskov JK (2007) Electroanal Chem 607:83
6. Lodi G, Sivieri E, De Battisti A, Trasatti S (1978) J Appl Electrochem 8:135
7. Jirkovský J, Hoffmannová H, Klementová M, Krtil P (2006) J Electrochem Soc 153:E111
8. Jirkovský J, Makarová M, Krtil P (2006) Electrochem Commun 8:1417
9. Macounová K, Jirka I, Trojánek A, Makarová M, Samec Z, Krtil P (2007) J Eletrochem Soc 154:A1077
10. Makarová M, Jirkovský J, Klementová M, Jirka I, Macounová K, Krtil P (2008) Electrochim Acta 53:2656
11. Macounová K, Makarova MV, Jirkovský J, Krtil P (2008) Electrochim Acta 53:6126